Article

Cell Reports

Direct Induction and Functional Maturation of Forebrain GABAergic Neurons from Human Pluripotent Stem Cells

Graphical Abstract

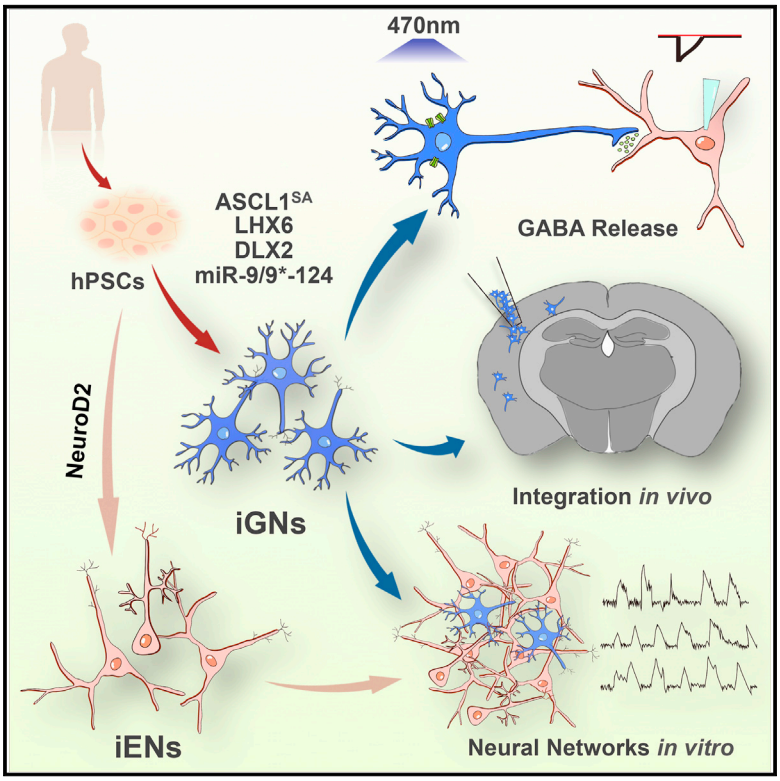

Authors

Alfred Xuyang Sun, Qiang Yuan, Shawn Tan, ..., Huck Hui Ng, Bing Lim, Hyunsoo Shawn Je

Correspondence

alfred_xy_sun@nni.com.sg (A.X.S.), shawn.je@duke-nus.edu.sg (H.S.J.)

In Brief

Sun et al. identify a combination of genetic factors that can directly transform hPSCs into forebrain GABAergic neurons with high efficiency. These induced neurons express canonical interneuron markers and exhibit mature functional properties, suggesting that they may be useful for neuronal subtype-specific studies and cortical network assembly.

Highlights

- We identify factors that directly induce GABAergic neurons (iGNs) from hPSCs
- iGNs express telencephalic interneuron markers and the subtype marker SST
- iGNs functionally mature, release GABA, and generate synaptic networks in vitro
- iGNs integrate into host synaptic circuits in vivo

Sun et al., 2016, Cell Reports *16*, 1942–1953
August 16, 2016
http://dx.doi.org/10.1016/j.celrep.2016.07.035

OPEN ACCESS
CellPress

Cell Reports
Article

Direct Induction and Functional Maturation of Forebrain GABAergic Neurons from Human Pluripotent Stem Cells

Alfred Xuyang Sun,[1,2,3,8,*] Qiang Yuan,[4,5,8] Shawn Tan,[4,5] Yixin Xiao,[4] Danlei Wang,[4] Audrey Tze Ting Khoo,[4] Levena Sani,[1] Hoang-Dai Tran,[2] Paul Kim,[4] Yong Seng Chiew,[4] Kea Joo Lee,[6] Yi-Chun Yen,[4] Huck Hui Ng,[2,5] Bing Lim,[1,9] and Hyunsoo Shawn Je[4,7,*]

[1]Cancer Stem Cell Biology, Genome Institute of Singapore, 60 Biopolis Street, Singapore 138672, Singapore
[2]Stem Cell and Regenerative Biology, Genome Institute of Singapore, 60 Biopolis Street, Singapore 138672, Singapore
[3]Department of Neurology, National Neuroscience Institute, 20 College Road, Singapore 169856, Singapore
[4]Molecular Neurophysiology Laboratory, Signature Program in Neuroscience and Behavioral Disorders, Duke-NUS Medical School, 8 College Road, Singapore 169857, Singapore
[5]Graduate School for integrative Sciences and Engineering, National University of Singapore, Singapore 117456, Singapore
[6]Department of Structure and Function of Neural Network, Korea Brain Research Institute, Daegu 701-300, Republic of Korea
[7]Department of Physiology, Yong Loo Lin School of Medicine, National University of Singapore, Singapore 117597, Singapore
[8]Co-first author
[9]Present address: Merck Research Laboratories, Translational Medicine Research Center, Singapore 138665, Singapore
*Correspondence: alfred_xy_sun@nni.com.sg (A.X.S.), shawn.je@duke-nus.edu.sg (H.S.J.)
http://dx.doi.org/10.1016/j.celrep.2016.07.035

SUMMARY

Gamma-aminobutyric acid (GABA)-releasing interneurons play an important modulatory role in the cortex and have been implicated in multiple neurological disorders. Patient-derived interneurons could provide a foundation for studying the pathogenesis of these diseases as well as for identifying potential therapeutic targets. Here, we identified a set of genetic factors that could robustly induce human pluripotent stem cells (hPSCs) into GABAergic neurons (iGNs) with high efficiency. We demonstrated that the human iGNs express neurochemical markers and exhibit mature electrophysiological properties within 6–8 weeks. Furthermore, in vitro, iGNs could form functional synapses with other iGNs or with human-induced glutamatergic neurons (iENs). Upon transplantation into immunodeficient mice, human iGNs underwent synaptic maturation and integration into host neural circuits. Taken together, our rapid and highly efficient single-step protocol to generate iGNs may be useful to both mechanistic and translational studies of human interneurons.

INTRODUCTION

GABAergic (GABA-secreting) interneurons are the principal elements that balance neural excitation within the brain (Markram et al., 2004). A major proportion of GABAergic interneurons in the cerebral cortex originate in the medial ganglionic eminence (MGE) of the developing ventral telencephalon and migrate tangentially into the neocortex (Bartolini et al., 2013; Nery et al., 2002; Pleasure et al., 2000; Wonders and Anderson, 2005). Given recent findings that the dysfunction of GABAergic interneurons may underlie diverse developmental and psychiatric disorders (Marín, 2012), the generation of high-purity GABAergic interneurons from human embryonic stem cells (hESCs) or patient-derived, induced pluripotent stem cells (hiPSCs) is desirable for mechanistic studies of GABAergic neuronal dysfunction and for drug discovery research. Accordingly, by mimicking the developmental signaling that occurs during ventral forebrain biogenesis, several groups have successfully derived MGE-like progenitors from hPSCs (hESCs and hiPSCs) and subsequently differentiated these progenitors into functional GABAergic neurons (Kim et al., 2014; Liu et al., 2013; Maroof et al., 2013; Nicholas et al., 2013). However, most of these methods involve multiple intermediate stages that require varying combinations of recombinant growth factors and small molecules and eventually yielded mixtures of both non-neuronal and neuronal cells with variable functional properties. The protracted timeline required to attain neuronal maturity and synaptic competence is a further limitation because this process can take as long as 30 weeks (Nicholas et al., 2013) (summarized in Table S1).

Ectopic expression of defined genetic elements has recently been shown to convert non-neuronal human cells into various neuronal subtypes (Caiazzo et al., 2011; Colasante et al., 2015; Son et al., 2011; Victor et al., 2014; Xu et al., 2015; Yoo et al., 2011; Zhang et al., 2013), offering an alternative method of generating desired cell types. Here, we describe the identification of three transcription factors (TFs), *ASCL1*, *DLX2*, and *LHX6*, that synergize with microRNA-9/9* and microRNA-124 to generate a highly enriched population of cells showing the characteristics of GABAergic interneurons (iGNs) from hPSCs. Our protocol can produce a large number of cells that exhibit genetic and neurochemical profiles similar to rodent

cortical interneurons with >80% efficiency. Significantly, we show that, within 6–8 weeks, the iGNs exhibit mature functional properties and form synapses either among themselves or with induced human glutamatergic excitatory neurons (iENs, which are generated by the forced expression of a single TF, *NEUROD2*). When transplanted into the cortex of immunodeficient mice, human iGNs matured and received synaptic currents from host neurons. To further illustrate the potential utility of our method, we monitored the network activity of microcircuits formed by the induced neurons in vitro under both basal and drug-challenged conditions using Ca^{2+} imaging and determined the cell-type-specific effects of a schizophrenia-linked gene, *MDGA1* (Lee et al., 2013). Our single-step, rapid, and robust method of generating induced human GABAergic neurons will likely be useful not only for modeling brain disorders that affect inhibitory neurons but also for cell-type-specific drug screening.

RESULTS

Identification of Genetic Elements that Directly Convert hPSCs to GABAergic Neurons

To identify genetic elements that can directly convert hESCs to GABAergic neurons, we focused on four TFs, *ASCL1*, *DLX2*, *NKX2.1*, and *LHX6*. These TFs are highly expressed in the MGE, a major site of GABAergic neurogenesis (Kessaris et al., 2014) and have been previously shown to be important for the differentiation and functional maturation of cortical interneurons (Figure 1A). Achaete-scute complex-like homolog 1 (*ASCL1*, also known as *MASH 1*) is a proneural basic helix-loop-helix (bHLH) factor that is widely expressed in the embryonic ventral brain, where it promotes the differentiation of neuronal progenitors into GABAergic interneurons (Long et al., 2009; Schuurmans and Guillemot, 2002). Distal-less homeobox 2 (*DLX2*) is a multifunctional TF that inhibits the differentiation of progenitors into glial cells and promotes their differentiation into GABAergic neurons (Anastasiades and Butt, 2011; Wonders and Anderson, 2005). NK2 homeobox 1 (*NKX2.1*) controls the migration of telencephalic interneurons and also determines the subtype identity of interneuron progenitors within the MGE (Anastasiades and Butt, 2011; Wonders and Anderson, 2005). LIM homeobox 6 (*LHX6*), which is a direct target of *NKX2.1*, is required for the fate-specification of MGE precursors into parvalbumin (PV)- or somatostatin (SST)-expressing cortical interneurons (Du et al., 2008; Neves et al., 2013).

We generated lentiviruses expressing each of the four TFs, infected hESCs (line H1), and assessed their conversion to neuronal cells by staining the cells for the pan-neuronal marker MAP2 at 10 days post-transduction (dpt) (Pang et al., 2011; Zhang et al., 2013) (Figure 1B). Initially, hESCs highly expressed pluripotency markers, such as OCT4, NANOG, and SOX2, but did not express neural progenitor markers NESTIN and MUSASHI (Figure S1A). Intriguingly, the expression of ASCL1 (indicated as A) alone converted 11.3% ± 0.8% of hESCs into MAP2-positive cells at 10 dpt, whereas the expression of the other TFs (DLX2 [D], LHX6 [L], and NKX2.1 [N]) failed to produce significant MAP2-positive signals (Figure 1C). Similar results were obtained following immunohistochemical staining for another neuronal marker βIII tubulin (Figure S1B). We subsequently tested all possible combinations of the D, N, and L TFs, but did not observe neuronal conversion (Figure S1C), indicating that ASCL1 plays an instructive role in converting hESCs to neurons, consistent with previous reports (Chanda et al., 2014; Pang et al., 2011).

A recent study reported that a phospho mutant form of ASCL1 (in which five serine residues are substituted with alanine, denoted A^{SA}) is more potent than the wild-type ASCL1 in the ectopic neural induction in *Xenopus* embryos and *trans*-differentiation of human fibroblasts to neurons (Ali et al., 2014). We therefore overexpressed A^{SA} in hESCs and found that it resulted in the production of ~2-fold more MAP2-positive neurons than A (Figure 1C). Based on these results, we decided to include A^{SA} as a neurogenic TF that is necessary to induce the differentiation of hESCs to GABAergic neurons.

Next, we asked if the addition of other factors could enhance neuronal conversion and, more specifically, GABAergic neuronal conversion. To that end, we transduced hESCs with different pools of lentiviruses that contained A^{SA} as an obligatory factor together with various combinations of the other three TFs (D, N, and L) and quantified MAP2- and GABA-positive cells at 10 dpt (Figure 1D). The majority of TF combinations significantly enhanced neuronal conversion over that produced by A^{SA} alone (Figure 1D). Remarkably, a subset of them also dramatically increased the efficiency of GABAergic neuronal conversion, with A^{SA}DL producing the highest percentage of GABA and MAP2 double-positive cells (69.1% ± 3.6%) (Figure 1D). Taken together, these results show that D and L synergized with A^{SA} to preferentially produce GABAergic neurons from hESCs.

To further improve the overall conversion efficiency, we co-expressed miR-9/9*-124, which we have previously found to increase neuronal conversion from non-neuronal cells (Yoo et al., 2011), together with the A^{SA}, D, and L. Strikingly, the addition of miR-9/9*-124 significantly increased the percentage of MAP2-positive cells from 50.3% ± 4.7% to 81.3% ± 3.1% (Figure 1E) while maintaining the high $GABA^+/MAP2^+$ ratio (Figure 1F). Moreover, the expression of miR-9/9*-124 enhanced dendritic arborization (Figure S1D), demonstrated by an increase in the total dendritic length and number of primary branches of converted neurons (Figure S1E). Importantly, similar increases in neuronal conversion efficiency were observed across multiple hPSC lines, including two human ESCs (H1 and H9) and three different human iPSCs (hiPSC1-3, Figures 1F and S1A). The neuronal conversion rate continued to rise, reaching more than 90% after 35 dpt across multiple cell lines (Figure S1F). On the other hand, transduction of hESCs with miR-9/9*-124 alone failed to induce neuronal cells (Figure S1G). These results led us to conclude that A^{SA}, D, L, and miR-9/9*-124 (A^{SA}DL + miR-9/9*-124) are optimal factors for the induction of GABAergic neurons from hPSCs.

To promote survival and functional maturation, we co-cultured cells that were transduced with A^{SA}DL + miR-9/9*-124 with primary rat glia. Immunostaining at 42 dpt revealed that the majority of the induced neuronal cells were GABAergic (84.5% ± 3.5%) (Figures 1G and 1H). Small percentages of the converted

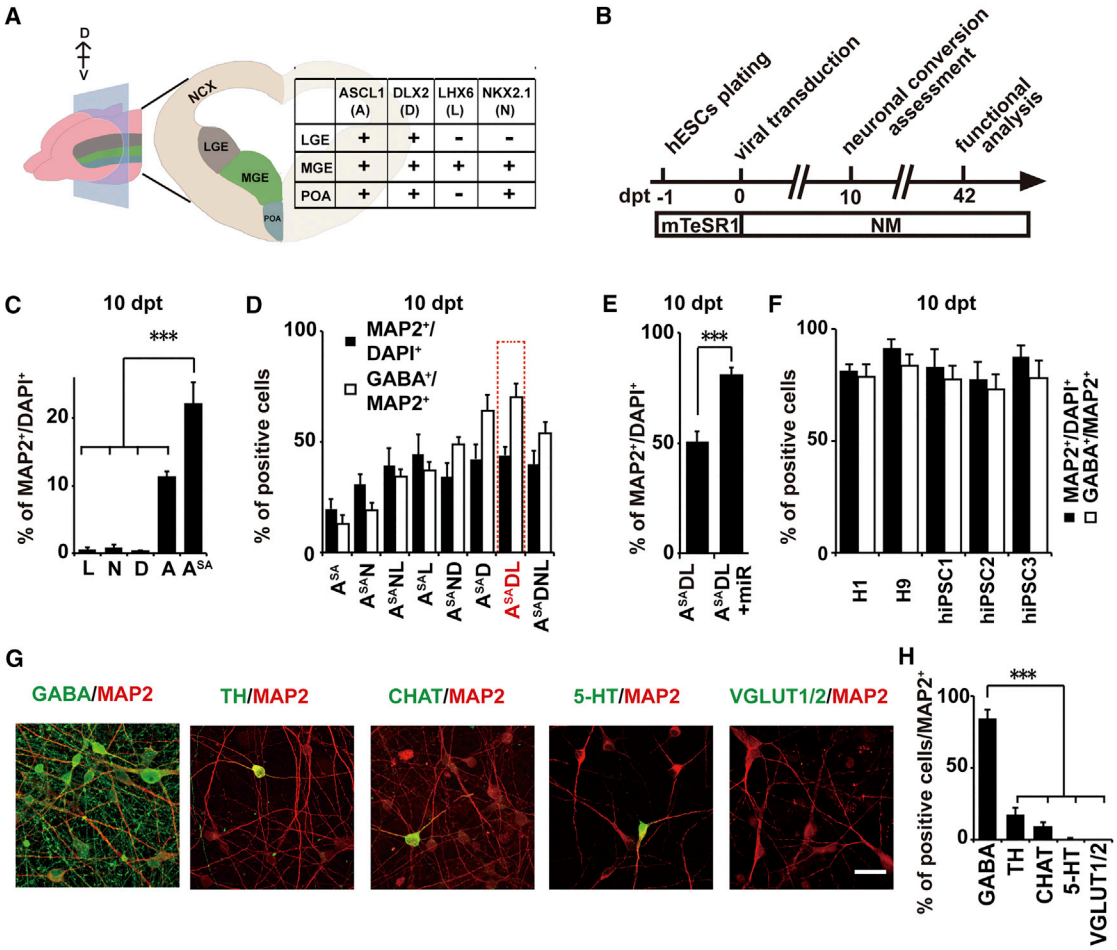

Figure 1. Identification of Genetic Elements that Efficiently Convert hPSCs to Induced GABAergic Neurons

(A) Schematic diagram illustrating expression of four genes (ASCL1, DLX2, NKX2.1, and LHX6) that are involved in genesis of cortical GABAergic neurons. D, dorsal; V, ventral; NCX, neocortex; LGE, lateral ganglionic eminence; MGE, medial ganglionic eminence; POA, preoptic area.

(B) An overview for direct induction of hESCs to neurons. One day after plating as single cells, hESCs were lentivirally transduced with various combinations of reprograming factors. Neuronal conversion of hESCs was typically assessed at 10 dpt, and detailed characterization of converted neurons was performed at 42 dpt or later. dpt, days post transduction; mTeSR1, hPSC media; NM, neuronal media.

(C) Efficiency of neuronal conversion of hESCs (line H1) at 10 dpt upon single transcription factor overexpression. The percentage of MAP2-positive cells over all cells (DAPI-positive) is shown (L, LHX6; N, NKX2.1; D, DLX2; A, ASCL1; ASA, ASCL1 phosphomutant). Data are means ± SEM (n > 3 independent experiments). One-way ANOVA followed by Tukey's test shows significant differences, ***$p < 0.001$.

(D) Efficiencies of pan-neuronal conversion (black bars) and GABAergic neuronal conversion (white bars) of hESCs (line H1) upon indicated TF combinations at 10 dpt. Data are means ± SEM (n = 3 independent experiments). The optimal combination, ASADL, is shown in red.

(E) Efficiency of neuronal conversion of ASADL-converted hESCs transduced with or without miR-9/9*-124 (shown as miR for simplicity throughout the manuscript) at 10 dpt. Data are means ± SEM (n > 3 independent experiments). Two-tailed, unpaired t test shows significant difference, ***$p < 0.001$.

(F) Efficiencies of pan-neuronal conversion (black bars) and GABAergic neuronal conversion (white bars) of two hESC lines (H1 and H9) and three hiPSC lines (iPSC1-3) by ASADL + miR at 10 dpt. Data are means ± SEM (n = 3 independent experiments).

(G and H) Representative images of H1 derived induced GABA-positive neuronal cells (iGNs) immunolabeled with MAP2 and markers of neuronal subtypes (GABA, gamma-aminobutyric acid; TH, tyrosine hydroxylase; CHAT, cholineacetyltransferase; 5-HT, 5-hydroxytryptamine [also known as serotonin]; VGLUT1/2, vesicular glutamate transporter 1 and 2). Data were collected at 42–50 dpt. Scale bar, 20 μm. The percentage of neuronal subtype marker-positive cells that also express neuronal marker MAP2 is shown in (H). Data are means ± SEMs (n = 3 independent experiments). One-way ANOVA followed by Tukey's test shows significant differences, ***$p < 0.001$.

neuronal cells expressed other neuronal markers, such as tyrosine hydroxylase (TH, a marker of dopaminergic neurons) and choline acetyltransferase (ChAT, a marker of cholinergic neurons) (Figures 1G and 1H). Virtually none of the converted neuronal cells expressed markers for excitatory glutamatergic neurons, such as vesicular glutamate transporter 1 and 2 (VGLUT1/2), or the marker for serotonergic neurons 5-hydroxytryptamine (5-HT) (Figures 1G and 1H). Taken together, these results demonstrate that the expression of $A^{SA}DL$ + miR-9/9*-124 could robustly induce hPSCs to differentiate into a relatively homogenous population of GABA-producing neuronal cells (namely, iGNs).

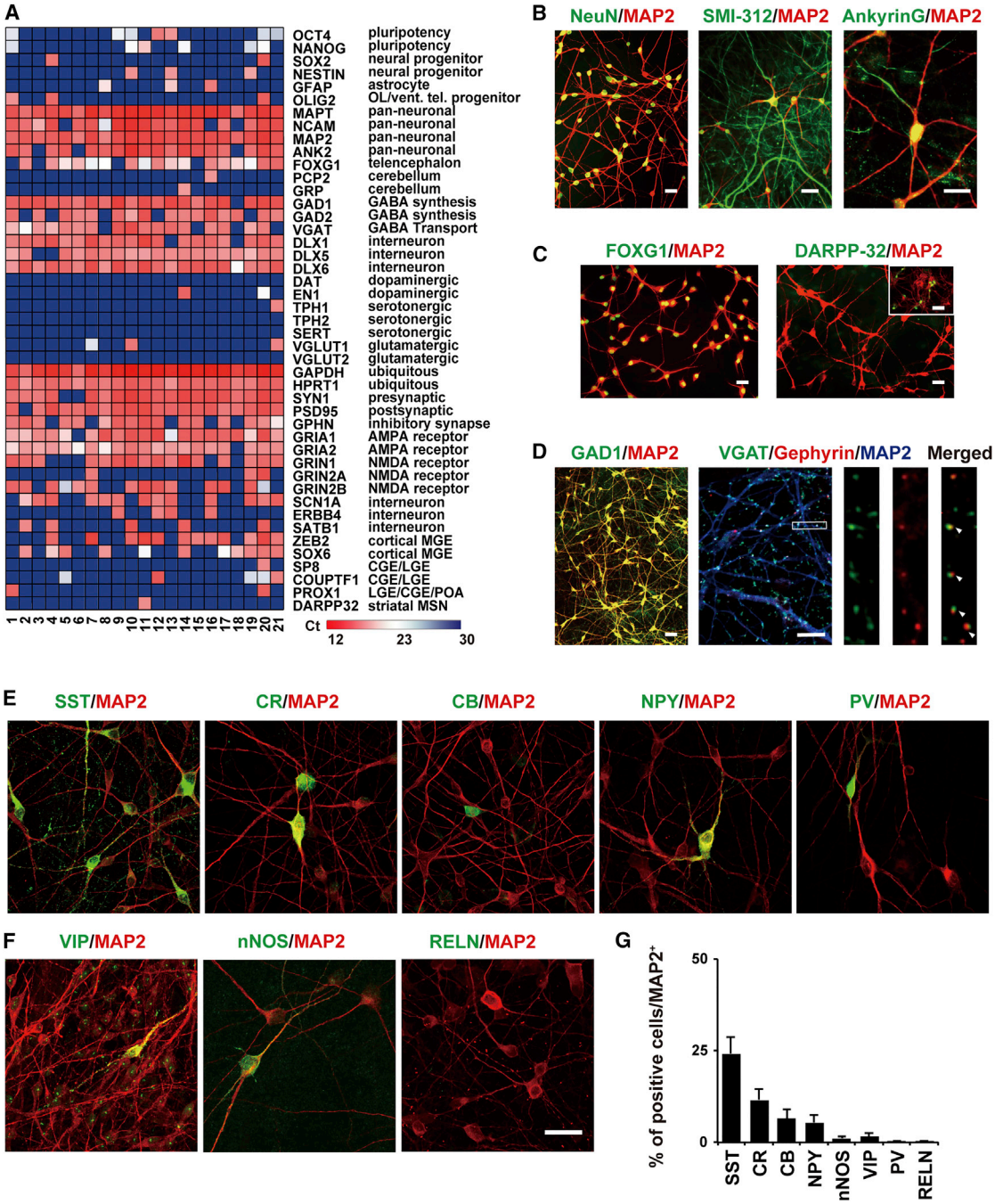

Figure 2. Expression of Forebrain Interneuronal Markers in iGNs

(A) qRT-PCR using Fluidigm Biomark platform, performed on cytoplasm aspirated from single iGN cells via a patch pipette. iGNs derived from H1 hESCs by overexpressing ASADL + miR-9/9*-124 were collected at 48–52 dpt. Expression levels (shown as Ct values) are color-coded at the bottom. Genes analyzed are indicated on the right with their cellular functions. Numbers indicate individual iGN cells analyzed.

(B) Immunostaining of iGNs with antibodies against NeuN (left, a mature neuronal marker), SMI-312 (middle, an axonal marker), and Ankyrin G (right, a marker for axon-initiating segment). Scale bar, 20 μm.

(C) iGNs expressed the telencephalic marker FOXG1 (left) but not DARPP-32 (right), a marker of striatal MSNs. Scale bar, 20 μm. The inset inside the right panel showed positive signal of DARPP-32 antibody on cultured rat striatal neurons, which are known to contain DARPP-32 expressing MSNs. Inset scale bar, 60 μm.

(D) Left: representative image of iGNs stained with GAD1 antibody (GABA synthesis enzyme). Right: confocal image of iGNs stained with antibodies against the vesicular GABA transporter VGAT, the inhibitory postsynaptic protein Gephryin, and the neuronal marker MAP2. Scale bar, 20 μm. The inset was magnified on the right to show the juxtaposed bouton-like signals of VGAT and Gephyrin illustrating morphological inhibitory synapses.

(legend continued on next page)

Molecular Characterization of Human-Induced GABAergic Neurons

To gain insight into the kinetics of how iGNs acquire an inhibitory neuronal fate, we measured mRNA levels of key genes responsible for the GABAergic phenotype (*VGAT*, *GAD1*, and *GAD2*) in iGNs using qRT-PCR at 14 and 35 dpt. At 14 dpt, the iGNs expressed all three markers at levels similar to those observed in fetal human brains, which contained ~10%–15% GABAergic interneurons (Figure S2A). By 35 dpt, the expression of all three genes markedly increased (a 6- to 13-fold increase), indicating further maturation of the iGNs (Figure S2A).

To further characterize the iGNs, we performed multiplexed gene expression analysis of single iGNs at 48–52 dpt (Figure 2A; Table S2). We noted a drastic erasure of pluripotency markers (*OCT4* and *NANOG*) with concurrent uniform expression of pan-neuronal markers (*MAPT*, *NCAM*, *MAP2*, and *ANK2*) (Figure 2A). The expression of markers of neural progenitors (*SOX2* and *NESTIN*), astrocytes (*GFAP*), and oligodendrocytes (*OLIG2*) was negligible (Figure 2A). The iGNs expressed the telencephalic marker *FOXG1* but not *PCP2* and *GRP*, which are genes that are highly expressed in the cerebellum. Furthermore, consistent with the immunostaining data, markers of GABAergic interneurons (*GAD1*, *GAD2*, *VGAT*, *DLX1*, *DLX5*, and *DLX6*) were expressed in virtually all cells, whereas the expression of markers indicative of other neuronal lineages were largely absent (dopaminergic: *DAT* and *EN1*; serotonergic: *TPH1*, *TPH2*, and *SERT*; glutamatergic: *VGLUT1* and *VGLUT2*) (Figure 2A). The majority of the iGNs robustly expressed synaptic markers (*SYN1*, *PSD95*, and *GPHN*) as well as AMPA and NMDA receptors (*GRIA1*, *GRIA2*, *GRIN1*, *GRIN2A*, and *GRIN2B*). They also expressed genes that have been previously shown to be important for the function of interneurons, such as *SCN1A*, *ERBB4*, and *SATB1* (Figure 2A). Finally, many iGNs expressed cortical, MGE-derived interneuronal markers such as *ZEB2* and *SOX6*. However, the majority of iGNs did not express *SP8*, *COUPTF1*, or *PROX1*; markers of interneurons with alternative birthplaces (CGE, LGE, and POA); or *DARPP-32*, a defining marker of striatal medium spiny neurons (MSNs). Collectively, these data indicate that the iGNs comprised a highly enriched population of cortical GABAergic neurons.

To corroborate the mRNA expression data, we performed immunostaining analyses of the iGNs. The iGNs strongly expressed NeuN, a mature neuronal marker, the axonal marker SMI-312 and Ankyrin G, an axon initial segment marker (Figure 2B). Not surprisingly, the majority of the iGNs stained positive for FOXG1, a forebrain marker, but were negative for DARPP-32, a marker of MSNs (Figure 2C). Consistent with the GABAergic nature of the induced cells, GAD1 was readily detected in the iGNs (Figure 2D). Importantly, we observed that gephyrin-positive puncta were juxtaposed to VGAT-positive puncta along the dendrites of the iGNs, providing a morphological indication of GABAergic synapses (Figure 2D).

Mature cortical interneurons can be divided into different subgroups based on their expression of neuropeptides and calcium-binding proteins, including SST, PV, calretinin (CR), calbindin (CB), neuropeptide Y (NPY), reelin (RELN), neuronal nitric oxide synthetase (nNOS), and vasoactive intestinal peptide (VIP) (Kepecs and Fishell, 2014; Markram et al., 2004; Miyoshi and Fishell, 2011; Ascoli et al., 2008). Immunostaining revealed that a subset of iGNs expressed SST (24.3% ± 4.6%), CR (11.6% ± 3.0%), CB (6.5% ± 2.4%), and NPY (5.4% ± 2.0%) (Figures 2E and 2G). We found that ~10% of $MAP2^+$ cells were double-positive for SST and CR (Figure S2B), while SST and CB double-positive cells were not present. PV-positive signals could only be consistently observed after 70 dpt, albeit in a small number of the iGNs (<1%, 5 out of 576 neurons) (Figures 2E and 2G). We further examined other GABAergic subtype markers, including VIP (1.5% ± 1.0%), nNOS (1.1% ± 0.6%), and RELN (<1%) (Figures 2F and 2G), and found them to be scarcely present. Immunostaining analysis in iGNs converted from another hiPSC line (hiPSC3) exhibited similar interneuronal subtype distributions (Figure S2C), and we observed comparable percentages of SST-expressing iGNs across multiple hPSC lines (Figure S2D), indicating that our protocols could produce iGNs from multiple hPSC lines with similar conversion efficiency and comparable subtype distribution.

Functional Characterization of Induced GABAergic Neurons

To explore whether the iGNs exhibited functional membrane properties similar to those of neurons, we performed patch-clamp recordings of iGNs at 42 and 56 dpt. In voltage-clamp mode, the iGNs showed fast inactivating inward and outward currents, which likely corresponded to the opening of voltage-dependent potassium (K^+)- and sodium (Na^+)-channels, respectively (Figure 3A). The peaks of the voltage-gated Na^+ and K^+ currents increased significantly from 42 to 56 dpt (Figure 3B). Consistent with this finding, we observed a significant decrease in membrane resistance (Rm), a significant increase in membrane capacitance (Cm), and a more hyperpolarized resting membrane potential (RMP), indicating that iGNs were more mature at 56 dpt (Figure 3C; Table S3). These data show that the iGNs possessed the fundamental structural components required to function as neurons.

Next, both spontaneous and elicited action potentials (APs) were recorded from iGNs in cell-attached mode (Figure 3D) and in current-clamp mode (Figures 3E and 3F), respectively. Upon current injection, iGNs at 56 dpt showed enhanced AP firing (Figure 3F). We performed electrophysiological recordings from iGNs derived from additional cell lines (H9 and hiPSC1) and observed similar results (Figures S2E–S2H). We then further characterized the iGNs based on their AP firing patterns. When the iGNs were grouped based on their AP firing, the majority displayed an accommodating pattern (type I, 47%) or

(E) Immunostaining of iGNs with antibodies against interneuronal subtype markers, including somatostain (SST), calretinin (CR), calbindin (CB), and neuropeptide-Y (NPY), and parvalbumin (PV). Data were collected between 42–56 dpt, except for PV, which was collected at 70–90 dpt. Scale bar, 20 μm.
(F) Immunostaining of iGNs with antibodies against interneuronal subtype markers, including Reelin (RELN), neuronal nitric oxide synthetase (nNOS), and vasoactive intestinal peptide (VIP). Arrowheads point to neuronal cells that also expressed subtype makers as indicated. Scale bar, 20 μm.
(G) Quantification of percentage of interneuronal subtype markers shown in (E) and (F) as a bar graph. Data are means ± SEM (n = 3 independent experiments).

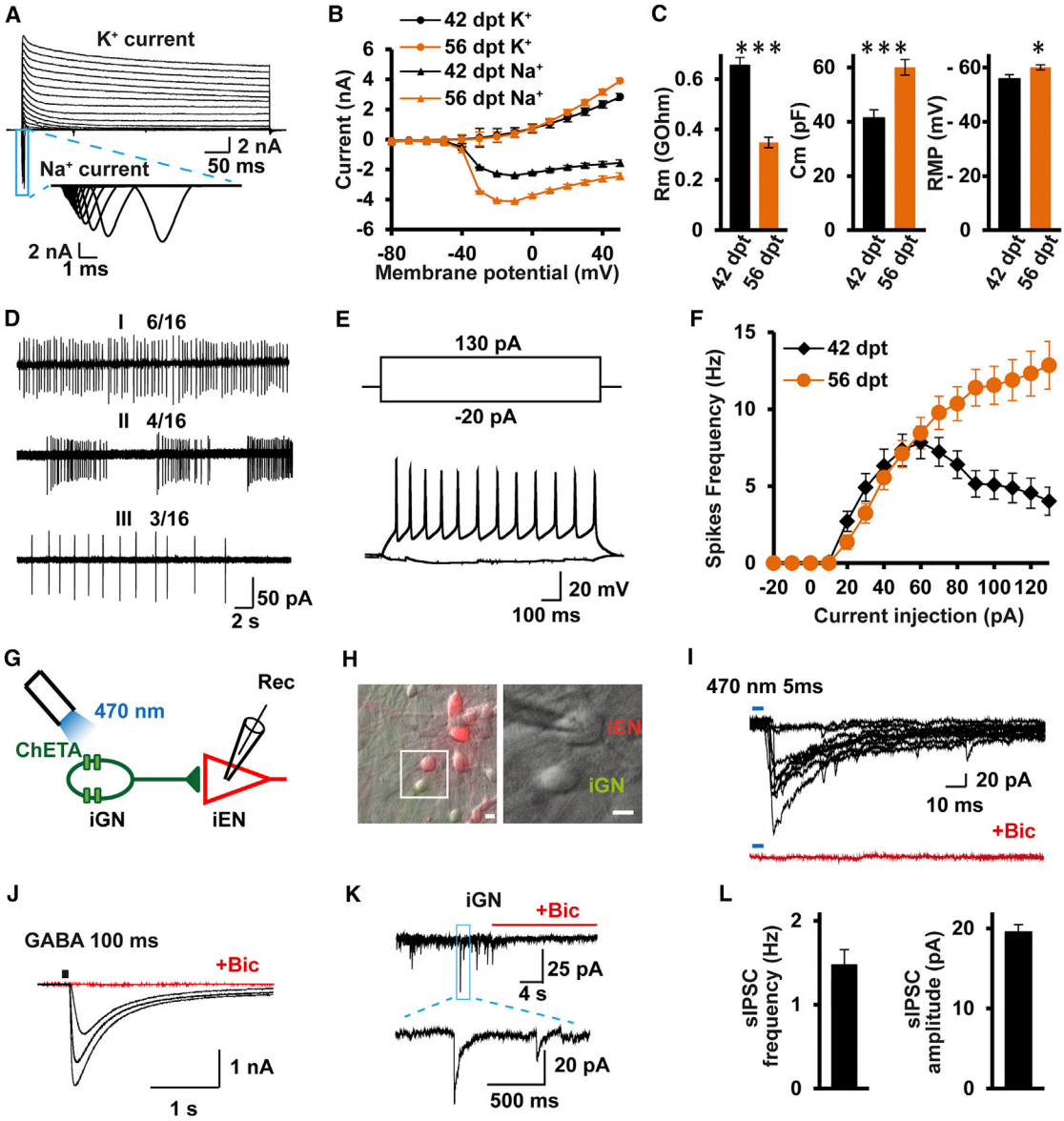

Figure 3. Electrophysiological Properties of iGNs Induced from hESCs

(A–F) Intrinsic electrophysiological properties of iGNs. (A) Representative traces showing the presence of voltage-dependent Na^+ and K^+ currents in iGNs. Blue box points to Na^+-channel-dependent inward current. (B) Averaged (means ± SEM) current-voltage relationship (I/V curves) for Na^+ and K^+ currents, recorded from iGNs at either 42 dpt (n = 41) or 56 dpt (n = 53). (C) Quantification of membrane resistance (Rm, left), membrane capacitance (Cm, middle), and resting membrane potential (RMP, right) recorded from iGNs at either 42 dpt (n = 41) or 56 dpt (n = 53). Statistical significance was assessed by two-tailed, unpaired t test (*$p < 0.05$, **$p < 0.01$, ***$p < 0.001$). (D) Representative traces of different patterns of spontaneous action potentials (APs), recorded from iGN at 56 dpt under cell-attached mode. Total number of cells analyzed: n = 16. (E) Representative trace of multiple APs generation (the lower panel) recorded from iGN at 56 dpt triggered by current injection (the upper panel). (F) Characterization of APs generation properties in terms of spikes frequency with current-pulse amplitude, recorded from iGNs at either 42 dpt (n = 41) or 56 dpt (n = 53).

(G–L) Demonstration of GABA release from iGNs. (G) Schematic diagram showing the patching on an induced excitatory neuron (iEN) that is synaptically connected with a ChETA-expressing iGN. (H) Merged differential interference contrast (DIC) and fluorescence (EYFP labels iGNs and turboRFP labels iENs) images of induced neurons for optogenetics. The image on the right depicts selecting patching on iEN, enlarged from the left image. Scale bar, 5 μm. (I) Upper panel: overlaid traces showing synaptic responses (upper panel) evoked by repeated presynaptic optogenetic stimuli (5 ms every 30 s, showed as blue light) in iGNs. Only two out of ten stimuli failed to trigger IPSCs. Lower panel: addition of bicuculline (20 μM) completely blocked the evoked response. (J) Exogenous GABA (1 mM, 100 ms)-evoked response (black trace) recorded from iGN. This response was blocked by bicuculline treatment (red trace). (K) Representative traces of spontaneous IPSCs (sIPSCs) recorded in iGN, which are blocked by bicuculline. A blue box illustrated details of sIPSCs. (L) Quantification of sIPSC frequency (left) and amplitude (right) recorded from iGNs at 42–56 dpt (n = 61).

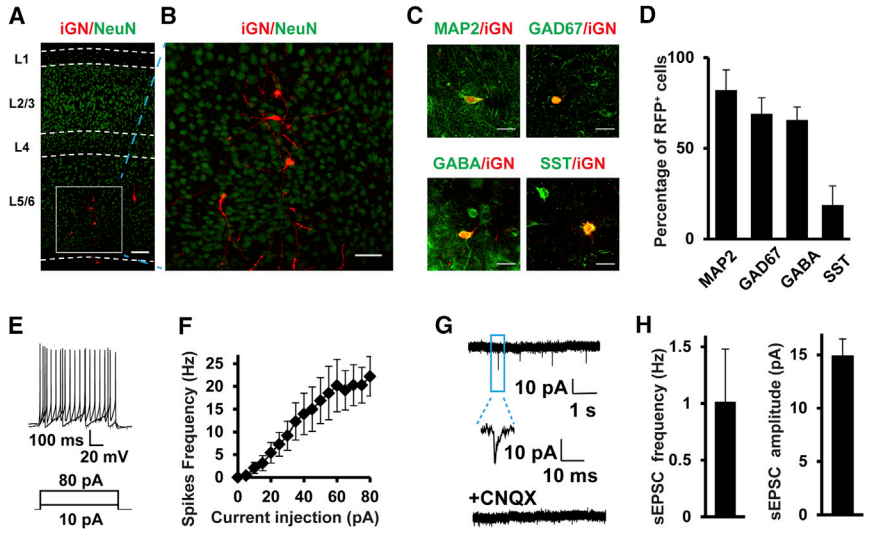

Figure 4. Functional Maturation and Integration of Transplanted Human iGNs in the Mouse Cortex

(A) An overview to illustrate the dispersion of human iGNs (red) in the mouse cortex, mostly in layer 5/6. Scale bar, 100 μm. The white box is magnified three times and is shown in (B).

(B) An illustration of the neurite arborization of the human iGNs (red). Human iGNs also expressed the mature neuronal marker NeuN. Scale bar, 50 μm.

(C) Transplanted human iGNs expressed the pan-neuronal marker MAP2, GABAergic markers GAD67 and GABA, and interneuron subtype marker SST. Scale bar, 20 μm. Quantifications of the percentage of human cells positive for each marker is shown in (D). Data were obtained from n = 3 animals, with more than 20 cells counted for each marker.

(E) Representative trace of multiple APs generation (the lower panel) recorded from transplanted human iGN triggered by current injection (the lower panel).

(F) Characterization of APs generation properties of human iGNs in terms of spikes frequency with current-pulse amplitude.

(G) Representative traces of spontaneous EPSCs (sEPSCs) recorded in iGN, which are blocked by CNQX (50 μM). A blue box illustrated details of sEPSCs.

(H) Quantification of sEPSC frequency (left) and amplitude (right) recorded from iGNs (n = 9). Data are shown as the mean ± SEMs.

non-accommodating pattern (type II, 38%), whereas anti-accommodating (type III, 6%) and single AP firing (type IV, 9%) patterns were also observed in small subsets of the iGNs (Figures S2I and S2J). These observations are consistent with previous studies that showed that the AP firing of the majority of SST-positive neurons in the neocortex typically displays an accommodating pattern (Wang et al., 2002). We did not detect any fast-spiking or bursts of APs in the recordings from iGNs (data not shown). However, we found that the non-accommodating iGNs exhibited a greater firing frequency and larger AHP compared to the accommodating iGNs (Figures S2K and S2L). Furthermore, small current injections (<70 pA) induced more frequent AP firing in type I cells than in type II cells, but the type II cells fired more APs in response to larger current injections (>100 pA) (Figure S3L). Taken together, these data indicate that the iGNs displayed different types of AP firing patterns, similar to cortical interneurons.

Next, to further confirm that the iGNs expressed the functional presynaptic machinery needed to release GABA and induce inhibitory postsynaptic responses, we co-cultured iGNs with iENs that were generated with a protocol similar to that used in a previous study (Zhang et al., 2013) (Figures S3A–S3F). First, we expressed ChETA, an engineered channelrhodopsin variant (Gunaydin et al., 2010), only in iGNs; then, we stimulated the ChETA-expressing iGNs with an optical fiber coupled to a high-intensity blue light-emitting diode (LED) (Figures 3G and 3H) (Campagnola et al., 2008). Blue LED illumination (470 nm) induced ChETA-mediated inward currents and AP firing in iGNs while the same photostimulation did not induce such currents in neurons that did not express ChETA, demonstrating that the iGNs could be selectively activated using this approach (Figures S3G–S3L). Under these conditions, short pulses of photostimulation that activated the ChETA-expressing iGNs induced postsynaptic responses in iENs (Figure 3I). The recorded postsynaptic currents showed short synaptic delays, indicating that they were induced monosynaptically (Figure 3I). Moreover, these light-evoked synapse responses were completely abolished by bicuculline, a $GABA_A$ receptor antagonist (Figure 3I). These results indicated that the activation of iGNs generated inhibitory postsynaptic responses in co-cultured iENs.

We further investigated whether the iGNs exhibited functional postsynaptic mechanisms, which would enable synaptic transmission in situ. First, exogenous application of GABA (1 mM, 100 ms) triggered inhibitory postsynaptic currents (IPSCs) in iGNs (Figure 3J). These iPSCs were also completely blocked by bicuculline, indicating that the iGNs expressed functional $GABA_A$ receptors (Figure 3J). Second, at 42–56 dpt, the majority of the iGNs showed spontaneous inhibitory postsynaptic currents (sIPSCs) at a mean frequency of 1.47 ± 0.18 Hz with an amplitude of 19.5 ± 1.38 pA (Figures 3K and 3L, n = 61). These sIPSCs were completely abolished by bicuculline (Figure 3K), indicating that the human iGNs possessed functional postsynaptic machinery and received inhibitory synaptic inputs.

Functional Maturation and Synaptic Integration of Human iGNs In Vivo

To test whether the iGNs were able to undergo synaptic maturation and functional integration in vivo, we stereotaxically transplanted RFP-expressing iGNs at 8 dpt into cortices of P1 neonatal immunodeficient NOD SCID mice (Ideguchi et al., 2010; Espuny-Camacho et al., 2013; Gaspard et al., 2008). Two months later, NeuN expressing iGNs were dispersed in mouse cortex, mostly in layer 5/6 (Figures 4A and 4B). Quantification revealed that majority of the iGNs was positive for neuronal marker MAP2 and GABAergic markers GAD67 and GABA, indicating successful establishment of GABAergic neuronal identity (Figures 4C and 4D). Approximately 20% of transplanted iGNs expressed SST. These results are consistent

with our quantifications with cultured iGNs, indicating that our protocol primarily yielded SST^+ interneurons.

To determine whether transplanted iGNs could develop into functional neurons and integrate into host neural circuitry, we used whole-cell patch-clamp recordings in acute cortical slices obtained from transplanted mice. Grafted iGNs, identified by RFP expression, displayed repetitive AP firings (Figures 4E and 4F). Furthermore, we could measure spontaneous excitatory postsynaptic currents at −70 mV in voltage-clamp mode from transplanted iGNs in acute cortical slices and these synaptic currents were abolished in the presence of CNQX, an AMPA/kainate-type glutamate receptor antagonist (Figures 4G and 4H). To further confirm the functional synapse formations between host and transplanted iGNs, we performed ultrastructural analysis using serial block face-scanning electron microscopy (SBF-SEM) (Briggman et al., 2011). Examination of cortical area in brain slices immunostained with diaminobenzidine (DAB) for RFP showed synaptic connections onto grafted iGNs (Figures S3M–S3O). These results demonstrate that the transplanted human iGNs are electrically excitable and are able to integrate into host neural circuitry by forming functional synapses.

Potential Use of iGNs in Large-Population Calcium Imaging and Interneuron-Specific Mechanistic Studies

To explore the potential use of the iGNs to assess cell-type-specific drug effects or to model human disease states, we tested whether iGNs could form functional synaptic connections with other excitatory glutamatergic neurons. We co-cultured iGNs (20%) with iENs (80%), which mimics the proportions found in mammalian cortical networks, and measured spontaneous PSCs from the iGNs (Figure 5A). Intriguingly, when neurons were clamped at −70 mV, we could measure two distinct patterns of PSCs (Figures 5B and 5C). Treatment with bicuculline eliminated the slow-decay PSCs that resembled sIPSCs, and additional treatment with CNQX, an AMPA/kainate-type glutamate receptor antagonist, completely abolished the remaining fast-rise, fast-decay PSCs that most likely corresponded to AMPA receptor-mediated PSCs (Figures 5B and 5C). These data indicate clearly that the iGNs could form functional synaptic connections with other excitatory glutamatergic neurons.

Next, we examined spontaneous activity-dependent Ca^{2+} transients in either homogenous populations of iENs or in mixtures of 80% iENs and 20% iGNs. In a homogenous population of iENs, the addition of bicuculline did not affect the network activity, as measured by the synchronization of individual Ca^{2+} transients (Figures 5D and 5F; Movie S1). Intriguingly, in a mixed population of iENs and iGNs, the addition of bicuculline increased the synchronization of the activity of the overall network by increasing the frequency of bursts of Ca^{2+} transients with a higher degree of synchronization (Figures 5E and 5F; Movie S2), indicating that bicuculline removed the inhibitory influence of the iGNs within the neuronal network. This result was consistent with previous studies of cultured rodent neurons (Patel et al., 2015). These Ca^{2+}-imaging data demonstrate the potential use of iGNs in conjunction with iENs to monitor the spontaneous network activity of large populations of cells during drug screens.

Moreover, we tested whether the iGNs could be used for interneuron-specific mechanistic studies. Previously, we found that the overexpression of MAM-domain-containing glycosylphosphatidylinositol anchors 1 (MDGA1), which has been linked to autism and schizophrenia, in cortical neurons reduced inhibitory synapse numbers (Lee et al., 2013). However, whether the overexpression of MDGA1 in excitatory neurons or inhibitory neurons resulted in the reduced inhibitory synaptic input remained unclear. To this end, we expressed MDGA1 in a homogenous population of iGNs via lentiviral transduction and measured inhibitory synapse density based on the number of VGAT-positive clusters. We observed that overexpression of MDGA1 significantly reduced inhibitory synapse density (Figures 5G and 5H). Furthermore, compared with control cells, the iGNs that expressed MDGA1 displayed a significant reduction in sIPSC frequency (but not amplitude) (Control: 1.71 ± 0.29 Hz, MDGA1: 0.92 ± 0.25 Hz, $p < 0.05$; Control: 20.1 ± 1.58 pA, MDGA1: 16.66 ± 1.38 pA) (Figures 5I–5K). In contrast, the expression of MDGA1 in iENs (MDGA1 was overexpressed to similar levels in both iENs and iGNs, Figure S4A) did not affect excitatory synaptic transmission, as assessed by sEPSCs (Figures S4B–S4D). Together, these results indicate that MDGA1 overexpression specifically and autonomously affected interneuron synapses; thus, our iGNs may enable cell-type-specific mechanistic studies of genes.

DISCUSSION

In the present study, we described a single-step, efficient, and reproducible method of generating a population of human forebrain GABAergic neuronal cells (iGNs) based on the overexpression of selected genetic factors. Starting from hPSCs, we provided evidence that ASCL1, a proneural bHLH factor that is broadly expressed in the ventral brain, can induce a small fraction of MAP2-expressing neuronal cells within 7–10 days, consistent with previous reports (Figure 1C). Further attempts to increase the yield of GABAergic neurons led us to several interesting conclusions. First, we confirmed and extended an earlier finding that a phosphomutant of ASCL1 induced more neuronal cells in both *Xenopus* and human fibroblasts than its wild-type form (Ali et al., 2014). The underlying mechanism of the augmented neurogenic activity of A^{SA} in hESCs was not investigated in the current study. Second, co-expression of other factors, notably DLX2 and LHX6, together with A^{SA} significantly enhanced neuronal transformation while biasing the resultant neurons to differentiate almost exclusively into GABAergic interneurons. Earlier studies in which ASCL1 was ectopically expressed in rodent glia demonstrated that ASCL1 plays an instructive role in directing GABAergic neuronal fate (Heinrich et al., 2011), yet similar gain-of-function studies of human fibroblasts and hESCs reported the production of glutamatergic neurons (Chanda et al., 2014). Our results provide support for a proneural activity of ASCL1 and indicate that other factors such as DLX2 and LHX6 confer hPSC-derived neurons with a GABAergic fate when they are expressed in conjunction with ASCL1. Third, miR-9/9*-124 synergized with these TFs to generate GABAergic neurons more efficiently from either hESCs or hiPSCs (Figure 1E). In support of these observations, we could

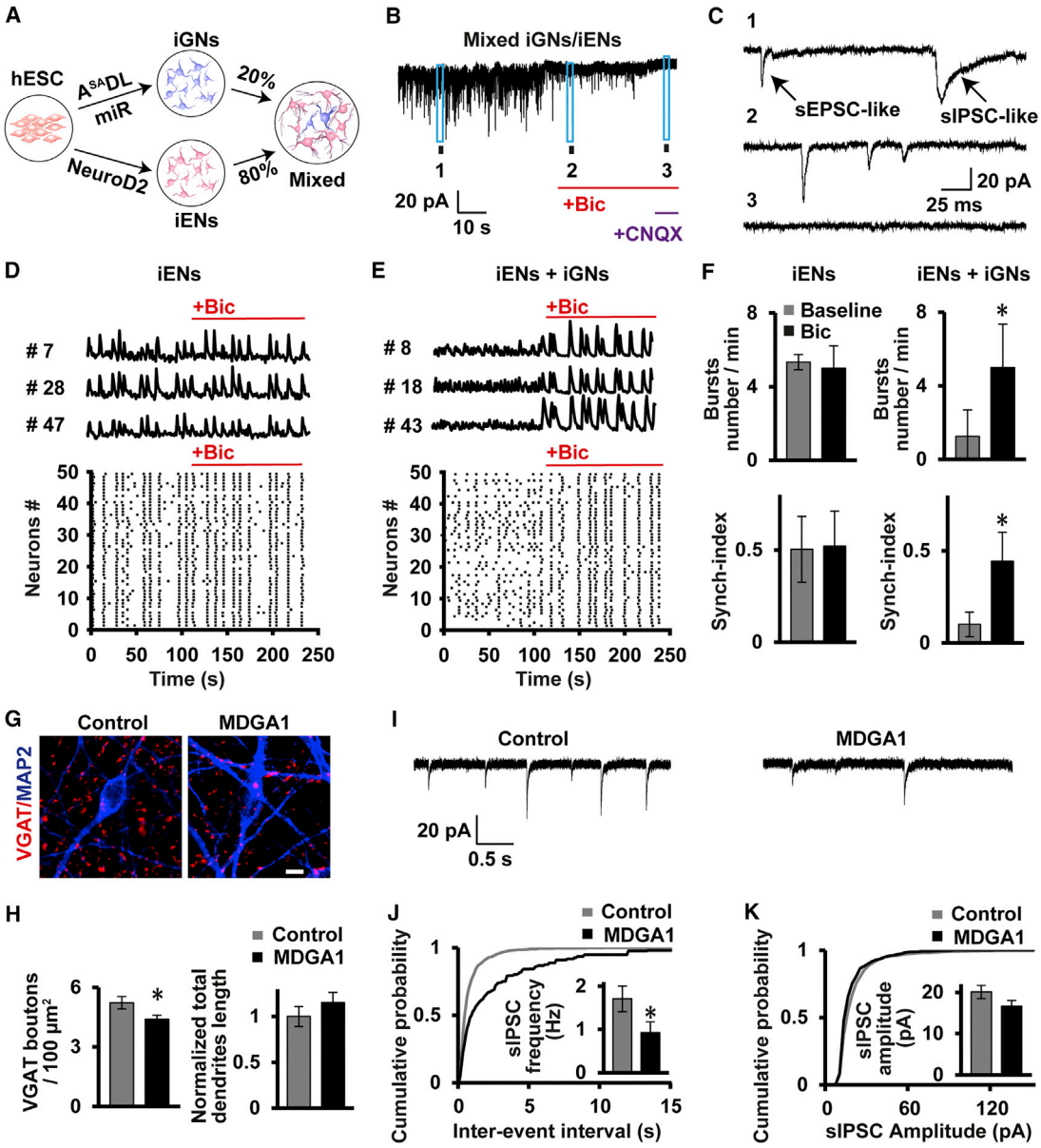

Figure 5. Applications of iGNs in Studies of Neural Network Activity and in Functional Interrogation of Gene Specifically Affecting Inhibitory Synapses

(A) Schematic diagram illustrating co-culture of human-induced excitatory (iEN, 80%) and inhibitory neurons (iGN, 20%) to mimic the ratio found in mammalian cortex. iGNs were generated by overexpression of ASADL + miR-9/9*-124 while iENs were generated by overexpression of NeuroD2.

(B) Both sIPSCs and sEPSCs were recorded from iGNs cultured on coverslips containing mixed iENs/iGNs, which are blocked by bicuculline and CNQX, respectively. Data were collected at 56 dpt.

(C) Zoomed-in traces for boxes 1–3 in (B).

(D and E) Representative raster plots of calcium spikes in iENs (D) or mixed iENs/iGNs network (E) with addition of bicuculline (indicated in red) after 2 min of baseline recording.

(F) Statistical analyses of bursts number (top) and synchronization index (bottom) of iENs (left) or mixed iENs/iGNs cultures (right) (n = 5 and 4 for iENs and mixed iENs/iGNs, respectively).

(G) Representative images of VGAT immunofluorescence staining of iGNs with control or MDGA1 overexpression. Scale bar, 5 µm.

(H) Quantification of VGAT positive bouton density, demonstrated by number of boutons over area of randomly chosen regions (left) with similar arborization of dendrites (right) (n = 8 for both control and MDGA1 overexpression).

(I) Representative traces of sIPSCs recorded in iGNs with control (left) or MDGA1 (right) overexpression.

(J and K) Cumulative plots and histograms of sIPSCs frequency (J) and amplitude (K) recorded in iGNs with control or MDGA1 overexpression (n = 13 and 12 for control and MDGA1 overexpression, respectively).

All histogram data are shown as the mean ± SEMs. Statistical significance was assessed by two-tailed, unpaired t test except for (F), two-tailed, paired t test, (*$p < 0.05$).

reliably generate GABAergic neurons from multiple types of hPSCs (Figures S1A and S2D) and could record mature neuronal properties in iGNs that were converted from additional hPSC lines (Figures S2E–S2H). Finally, we noted that although the iGNs appeared to uniformly express general forebrain GABAergic neuronal markers, multiple interneuronal subtypes were found that expressed SST, CR, CB, or NPY, with SST being the major subtype (Figures 2E, 2G, and S2C). Surprisingly, PV-positive neurons, a therapeutically important interneuron subtype that also originate from the MGE, were absent in our iGNs. Further studies are necessary to determine how to enrich specific interneuronal lineages, including PV-positive neurons.

Compared to previous attempts to derive GABAergic neurons from non-neuronal human cells, our method offers several advantages. First, our genetic gain-of-function approach bypasses the neural progenitor stage (see below, Figures S5C and S5G), thereby eliminating the need for various patterning factors and recombinant proteins. Second, our protocol generates functional iGNs within a significantly shorter period of time (6–8 weeks, compared to 10–30 weeks, Table S1), enabling more rapid turnaround of experiments. Third, our method primarily generates GABAergic neurons; few cells of other lineages are produced. These salient features enable a unique opportunity for in vitro assembly of microcircuits with neurons of defined identities and densities. Indeed, we observed distinct patterns of spontaneous neuronal network activity in dishes that contained discrete percentages of human excitatory (iENs) or inhibitory neurons (iGNs), and we recorded drug-induced alterations of the activity of the networks en bloc using Ca^{2+} imaging (Figures 5D–5F). These proof-of-principle experiments demonstrated clearly the feasibility in the utilization of such a system to interrogate the formation of more complex circuits and network behaviors.

Recently, Colasante et al. (2015) reported direct generation of GABAergic neurons from mouse and human non-neuronal cells through the overexpression of selected transcription factors. Compared to their protocol, we could achieve greater GABAergic neuronal conversion efficiency, probably due to inclusion of the phosphomutant of ASCL1 and microRNAs, despite similarity in some overlapping TFs. In addition, Colasante et al. (2015) utilized combination five TFs, of which two TFs must be silenced later in order to allow maturation to GABAergic neurons, while our protocol is single-step. The single-step nature of our method permitted us to generate a doxycycline (dox)-inducible iGN (as well as iEN) hESC line that can robustly differentiated into GABAergic neurons upon the addition of dox (Figure S5A). Dox-inducible iGN hESCs underwent drastic morphology changes within 6 days upon dox treatment (Figure S5A) and decreased proliferation, as revealed by reduced EdU incorporation (Figures S5F and S5J). These changes were concurrent with downregulation of pluripotency marker protein (OCT4) with converse upregulation of neuronal marker protein (MAP2) and later NeuN (Figures S5B and S5C). Intriguingly, we did not observe the expression of the neuropregenitor marker (NESTIN), indicating that dox-inducible iGN hESCs were directly differentiated into neuronal cells (Figures S5C and S5G). We further showed that dox-inducible direct differentiation of these hESCs did not elicit significant cell death (Figures S5D, S5E, S5H, and S5I). Thus, this single-step inducible cell line system, in contrast to conventional multi-stage differentiation protocols, can produce large quantities of functionally mature induced neurons within a shortened period of time, which makes it an attractive platform for high-throughput screenings.

Finally, our method enables neuronal subtype-specific characterization of the function of specific genes for disease modeling. For example, we found that the overexpression of MDGA1, a schizophrenia and bipolar disorder susceptibility gene (Li et al., 2011; Nagy, 2000; Pettem et al., 2013), in iGNs specifically reduced inhibitory synaptic transmission without altering excitatory synaptic transmission (Figures 5G–5K and S4). Previously, this cell-type-specific phenotyping was only achievable via the use of the Cre-lox system (Nagy, 2000), which requires the generation of specific Cre driver lines and floxed alleles or by the generation of fluorescence-based reporter cell lines and subsequent fluorescence-activated cell sorting (FACS)-mediated enrichment of specific cell types (DeRosa et al., 2015). Given the recent findings of the cell-type-specific effects of certain genetic risk variants in autism and schizophrenia, our method has great potential to enable both mechanistic and translation studies.

EXPERIMENTAL PROCEDURES

Plasmids Construction and Lentivirus Generation

We used a bi-cistronic lentiviral backbone as described (Addgene 31780) to clone cDNAs encoding hASCL1 (NM_004316.3), hASCL1-phosphmutant as described (Ali et al., 2014), hNKX2.1 (NM_003317.3), hDLX2 (NM_004405.3), hLHX6 (NM_014368.4), and hNeuroD2 (Addgene 31780) under the EF1a promoter, respectively. Doxycycline (Dox)-inducible lentiviral miR-9/9*-124 construct was as described (Addgene #31874). Lentiviral expression vector of rtTA was as described (Addgene 20342). For other constructs used in the study please refer to the Supplemental Experimental Procedures.

To generate lentiviral particles, lentiviral expression vectors together with psPAX2 and pMD2.G were co-transfected into Lenti-X 293T cells (Clontech) using Fugene HD (Roche) as described (Yoo et al., 2011). Supernatants were collected from culture media and lentiviral particles were concentrated using a PEG-it kit (LV810A-1, System Biosciences), following manufacture's protocol.

hPSCs Cell Cultures and Differentiation

All hPSC lines (hESCs, hiPSCs, and inducible iGN/iEN lines), which exhibit normal karyotypes, were maintained in mTeSR1 media (StemCell Technologies). Detailed information of the cell lines is described in the Supplemental Experimental Procedures. For differentiation, hPSCs were dissociated with TrypLE (Life Technologies) to single cells and subsequently plated onto tissue culture plates in mTeSR1 (Stem Cell Technologies), supplemented with ROCK inhibitor, thiazovivin (1 μM, Tocris). One day after plating, cells were transduced with lentiviruses expressing various genetic elements (as indicated in the study, day 0). Starting from 1 dpt, cells were maintained with Neuronal Media (Sciencell). For long-term culture, cells were replated at 7–10 dpt onto poly-L-lysine/laminin-coated glass coverslips for imaging, immunohistochemistry, and electrophysiology or onto tissue culture plates for gene expression analysis. Primary rat glial cells from P1 neonatal rat cortices were supplemented onto neuronal cells at 14–20 dpt to enhance survival and synaptic maturity of converted neuronal cells.

Immunocytochemistry

Immunofluorescence experiments were performed as previously described (Yoo et al., 2011) with antibodies listed in the Supplemental Experimental Procedures.

Gene Expression Analyses

For qRT-PCR analysis of pooled cultured cells, total RNA was extracted and mRNA levels were quantified by real-time PCR assay (Applied Biosystems 7900HT). For qRT-PCR analyses of single cells, cytoplasm from individual cell was aspirated with a patch pipette, and mRNA levels were measured using the Fluidigm Biomark dynamic array system as described (Pang et al., 2011).

Electrophysiology

Excitability and synaptic transmission of either iGNs or iENs were studied by whole-cell patch clamp in either voltage- or current-clamp mode. See also the Supplemental Experimental Procedures.

Optogenetic and Chemical GABA Evoked IPSC Recording

iGNs were transduced with Synapsin-ChETA-EYFP lentiviral particles and stimulated using blue (470 nm)-LED (Thorlabs, M470F1). Patch clamp recordings were performed in either co-cultured iENs or iGNs. Exogenous GABA (1 mM, Sigma) was applied using a picosplitzer (General Valve).

Calcium Imaging

Cells were stained with calcium indicator, Fluo-4 AM (ThermoFisher Scientific, F-14201) before confocal live-cell imaging. Images were acquired using LSM 710 (Zeiss) confocal microscopy using 20× objective at 37°C.

Statistical Analysis

Data were analyzed using the two-tailed unpaired or paired t test, or by one-way ANOVA followed by the post hoc Tukey's test.

SUPPLEMENTAL INFORMATION

Supplemental Information includes Supplemental Experimental Procedures, five figures, three tables, and two movies and can be found with this article online at http://dx.doi.org/10.1016/j.celrep.2016.07.035.

AUTHOR CONTRIBUTIONS

A.X.S. conceived, designed, and conducted experiments. Q.Y. designed and performed electrophysiological recordings, calcium imaging, and analyzed data. S.T. and Y.Y. performed stereotactic transplantations. Y.X. performed slice recordings. D.W., A.T.T.K., L.S., H.D.T., P.K., and Y.S.C. cultured and maintained neurons, acquired images, and performed imaging analyses. K.J.L. performed EM imaging. H.H.N., B.L, and H.S.J. supervised the project. A.X.S. and H.S.J. wrote the paper.

ACKNOWLEDGMENTS

We thank Drs. Junghyun Jo and Jaewon Ko for generously sharing reagents. We thank Judy Saw, Younghwan Lee, and Hidayat Bin Lokman O Mahat for providing technical support. We thank Drs. Wei Wu, Yishan Sun, and Carleton Goold for their assistance. We thank Drs. David Virshup and Wonkyung Ho for their critical reading of the manuscript. 3D-SEM images were acquired in the Advanced Neural Imaging Center at Korean Brain Research Institute (KBRI). This work was supported by Singapore Ministry of Education (MOE) Academic Research Fund (MOE2012-T2-1-021, MOE2014-T2-071), A*Star Translational Collaborative Research Partnership Grant (TCRP, 13/1/96/688), Singapore National Medical Research Council Research Grant (NMRC/CBRG/0075/2014), and Duke-NUS Signature Research Program Block Grant (to H.S.J.).

Received: November 11, 2015
Revised: April 12, 2016
Accepted: July 12, 2016
Published: August 4, 2016

REFERENCES

Ali, F.R., Cheng, K., Kirwan, P., Metcalfe, S., Livesey, F.J., Barker, R.A., and Philpott, A. (2014). The phosphorylation status of Ascl1 is a key determinant of neuronal differentiation and maturation in vivo and in vitro. Development *141*, 2216–2224.

Anastasiades, P.G., and Butt, S.J. (2011). Decoding the transcriptional basis for GABAergic interneuron diversity in the mouse neocortex. Eur. J. Neurosci. *34*, 1542–1552.

Ascoli, G.A., Alonso-Nanclares, L., Anderson, S.A., Barrionuevo, G., Benavides-Piccione, R., Burkhalter, A., Buzsáki, G., Cauli, B., Defelipe, J., Fairén, A., et al.; Petilla Interneuron Nomenclature Group (2008). Petilla terminology: nomenclature of features of GABAergic interneurons of the cerebral cortex. Nat. Rev. Neurosci. *9*, 557–568.

Bartolini, G., Ciceri, G., and Marín, O. (2013). Integration of GABAergic interneurons into cortical cell assemblies: lessons from embryos and adults. Neuron *79*, 849–864.

Briggman, K.L., Helmstaedter, M., and Denk, W. (2011). Wiring specificity in the direction-selectivity circuit of the retina. Nature *471*, 183–188.

Caiazzo, M., Dell'Anno, M.T., Dvoretskova, E., Lazarevic, D., Taverna, S., Leo, D., Sotnikova, T.D., Menegon, A., Roncaglia, P., Colciago, G., et al. (2011). Direct generation of functional dopaminergic neurons from mouse and human fibroblasts. Nature *476*, 224–227.

Campagnola, L., Wang, H., and Zylka, M.J. (2008). Fiber-coupled light-emitting diode for localized photostimulation of neurons expressing channelrhodopsin-2. J. Neurosci. Methods *169*, 27–33.

Chanda, S., Ang, C.E., Davila, J., Pak, C., Mall, M., Lee, Q.Y., Ahlenius, H., Jung, S.W., Südhof, T.C., and Wernig, M. (2014). Generation of induced neuronal cells by the single reprogramming factor ASCL1. Stem Cell Reports *3*, 282–296.

Colasante, G., Lignani, G., Rubio, A., Medrihan, L., Yekhlef, L., Sessa, A., Massimino, L., Giannelli, S.G., Sacchetti, S., Caiazzo, M., et al. (2015). Rapid conversion of fibroblasts into functional forebrain GABAergic interneurons by direct genetic reprogramming. Cell Stem Cell *17*, 719–734.

DeRosa, B.A., Belle, K.C., Thomas, B.J., Cukier, H.N., Pericak-Vance, M.A., Vance, J.M., and Dykxhoorn, D.M. (2015). hVGAT-mCherry: a novel molecular tool for analysis of GABAergic neurons derived from human pluripotent stem cells. Mol. Cell. Neurosci. *68*, 244–257.

Du, T., Xu, Q., Ocbina, P.J., and Anderson, S.A. (2008). NKX2.1 specifies cortical interneuron fate by activating Lhx6. Development *135*, 1559–1567.

Espuny-Camacho, I., Michelsen, K.A., Gall, D., Linaro, D., Hasche, A., Bonnefont, J., Bali, C., Orduz, D., Bilheu, A., Herpoel, A., et al. (2013). Pyramidal neurons derived from human pluripotent stem cells integrate efficiently into mouse brain circuits in vivo. Neuron *77*, 440–456.

Gaspard, N., Bouschet, T., Hourez, R., Dimidschstein, J., Naeije, G., van den Ameele, J., Espuny-Camacho, I., Herpoel, A., Passante, L., Schiffmann, S.N., et al. (2008). An intrinsic mechanism of corticogenesis from embryonic stem cells. Nature *455*, 351–357.

Gunaydin, L.A., Yizhar, O., Berndt, A., Sohal, V.S., Deisseroth, K., and Hegemann, P. (2010). Ultrafast optogenetic control. Nat. Neurosci. *13*, 387–392.

Heinrich, C., Gascón, S., Masserdotti, G., Lepier, A., Sanchez, R., Simon-Ebert, T., Schroeder, T., Götz, M., and Berninger, B. (2011). Generation of subtype-specific neurons from postnatal astroglia of the mouse cerebral cortex. Nat. Protoc. *6*, 214–228.

Ideguchi, M., Palmer, T.D., Recht, L.D., and Weimann, J.M. (2010). Murine embryonic stem cell-derived pyramidal neurons integrate into the cerebral cortex and appropriately project axons to subcortical targets. J. Neurosci. *30*, 894–904.

Kepecs, A., and Fishell, G. (2014). Interneuron cell types are fit to function. Nature *505*, 318–326.

Kessaris, N., Magno, L., Rubin, A.N., and Oliveira, M.G. (2014). Genetic programs controlling cortical interneuron fate. Curr. Opin. Neurobiol. *26*, 79–87.

Kim, T.G., Yao, R., Monnell, T., Cho, J.H., Vasudevan, A., Koh, A., Peeyush, K.T., Moon, M., Datta, D., Bolshakov, V.Y., et al. (2014). Efficient specification of interneurons from human pluripotent stem cells by dorsoventral and rostrocaudal modulation. Stem Cells *32*, 1789–1804.

Lee, K., Kim, Y., Lee, S.J., Qiang, Y., Lee, D., Lee, H.W., Kim, H., Je, H.S., Südhof, T.C., and Ko, J. (2013). MDGAs interact selectively with neuroligin-2 but not other neuroligins to regulate inhibitory synapse development. Proc. Natl. Acad. Sci. USA *110*, 336–341.

Li, J., Liu, J., Feng, G., Li, T., Zhao, Q., Li, Y., Hu, Z., Zheng, L., Zeng, Z., He, L., et al. (2011). The MDGA1 gene confers risk to schizophrenia and bipolar disorder. Schizophr. Res. *125*, 194–200.

Liu, Y., Liu, H., Sauvey, C., Yao, L., Zarnowska, E.D., and Zhang, S.C. (2013). Directed differentiation of forebrain GABA interneurons from human pluripotent stem cells. Nat. Protoc. *8*, 1670–1679.

Long, J.E., Cobos, I., Potter, G.B., and Rubenstein, J.L. (2009). Dlx1&2 and Mash1 transcription factors control MGE and CGE patterning and differentiation through parallel and overlapping pathways. Cereb. Cortex *19* (*Suppl 1*), i96–i106.

Marín, O. (2012). Interneuron dysfunction in psychiatric disorders. Nat. Rev. Neurosci. *13*, 107–120.

Markram, H., Toledo-Rodriguez, M., Wang, Y., Gupta, A., Silberberg, G., and Wu, C. (2004). Interneurons of the neocortical inhibitory system. Nat. Rev. Neurosci. *5*, 793–807.

Maroof, A.M., Keros, S., Tyson, J.A., Ying, S.W., Ganat, Y.M., Merkle, F.T., Liu, B., Goulburn, A., Stanley, E.G., Elefanty, A.G., et al. (2013). Directed differentiation and functional maturation of cortical interneurons from human embryonic stem cells. Cell Stem Cell *12*, 559–572.

Miyoshi, G., and Fishell, G. (2011). GABAergic interneuron lineages selectively sort into specific cortical layers during early postnatal development. Cereb. Cortex *21*, 845–852.

Nagy, A. (2000). Cre recombinase: the universal reagent for genome tailoring. Genesis *26*, 99–109.

Nery, S., Fishell, G., and Corbin, J.G. (2002). The caudal ganglionic eminence is a source of distinct cortical and subcortical cell populations. Nat. Neurosci. *5*, 1279–1287.

Neves, G., Shah, M.M., Liodis, P., Achimastou, A., Denaxa, M., Roalfe, G., Sesay, A., Walker, M.C., and Pachnis, V. (2013). The LIM homeodomain protein Lhx6 regulates maturation of interneurons and network excitability in the mammalian cortex. Cereb. Cortex *23*, 1811–1823.

Nicholas, C.R., Chen, J., Tang, Y., Southwell, D.G., Chalmers, N., Vogt, D., Arnold, C.M., Chen, Y.J., Stanley, E.G., Elefanty, A.G., et al. (2013). Functional maturation of hPSC-derived forebrain interneurons requires an extended timeline and mimics human neural development. Cell Stem Cell *12*, 573–586.

Pang, Z.P., Yang, N., Vierbuchen, T., Ostermeier, A., Fuentes, D.R., Yang, T.Q., Citri, A., Sebastiano, V., Marro, S., Südhof, T.C., and Wernig, M. (2011). Induction of human neuronal cells by defined transcription factors. Nature *476*, 220–223.

Patel, T.P., Man, K., Firestein, B.L., and Meaney, D.F. (2015). Automated quantification of neuronal networks and single-cell calcium dynamics using calcium imaging. J. Neurosci. Methods *243*, 26–38.

Pettem, K.L., Yokomaku, D., Takahashi, H., Ge, Y., and Craig, A.M. (2013). Interaction between autism-linked MDGAs and neuroligins suppresses inhibitory synapse development. J. Cell Biol. *200*, 321–336.

Pleasure, S.J., Anderson, S., Hevner, R., Bagri, A., Marin, O., Lowenstein, D.H., and Rubenstein, J.L. (2000). Cell migration from the ganglionic eminences is required for the development of hippocampal GABAergic interneurons. Neuron *28*, 727–740.

Schuurmans, C., and Guillemot, F. (2002). Molecular mechanisms underlying cell fate specification in the developing telencephalon. Curr. Opin. Neurobiol. *12*, 26–34.

Son, E.Y., Ichida, J.K., Wainger, B.J., Toma, J.S., Rafuse, V.F., Woolf, C.J., and Eggan, K. (2011). Conversion of mouse and human fibroblasts into functional spinal motor neurons. Cell Stem Cell *9*, 205–218.

Victor, M.B., Richner, M., Hermanstyne, T.O., Ransdell, J.L., Sobieski, C., Deng, P.Y., Klyachko, V.A., Nerbonne, J.M., and Yoo, A.S. (2014). Generation of human striatal neurons by microRNA-dependent direct conversion of fibroblasts. Neuron *84*, 311–323.

Wang, Y., Gupta, A., Toledo-Rodriguez, M., Wu, C.Z., and Markram, H. (2002). Anatomical, physiological, molecular and circuit properties of nest basket cells in the developing somatosensory cortex. Cereb. Cortex *12*, 395–410.

Wonders, C., and Anderson, S.A. (2005). Cortical interneurons and their origins. Neuroscientist *11*, 199–205.

Xu, Z., Jiang, H., Zhong, P., Yan, Z., Chen, S., and Feng, J. (2015). Direct conversion of human fibroblasts to induced serotonergic neurons. Mol. Psychiatry *21*, 62–70.

Yoo, A.S., Sun, A.X., Li, L., Shcheglovitov, A., Portmann, T., Li, Y., Lee-Messer, C., Dolmetsch, R.E., Tsien, R.W., and Crabtree, G.R. (2011). MicroRNA-mediated conversion of human fibroblasts to neurons. Nature *476*, 228–231.

Zhang, Y., Pak, C., Han, Y., Ahlenius, H., Zhang, Z., Chanda, S., Marro, S., Patzke, C., Acuna, C., Covy, J., et al. (2013). Rapid single-step induction of functional neurons from human pluripotent stem cells. Neuron *78*, 785–798.